TRACE Observation of Damped Coronal Loop Oscillations: Implications for Coronal Heating

V. M. Nakariakov,[1] L. Ofman,[2*] E. E. DeLuca,[3] B. Roberts,[1] J. M. Davila[4]

The imaging telescope on board the Transition Region and Coronal Explorer (TRACE) spacecraft observed the decaying transversal oscillations of a long [(130 ± 6) × 10^6 meters], thin [diameter (2.0 ± 0.36) × 10^6 meters], bright coronal loop in the 171 angstrom Fe^{IX} emission line. The oscillations were excited by a solar flare in the adjacent active region. The decay time of the oscillations is 14.5 ± 2.7 minutes for an oscillation with a frequency 3.90 ± 0.13 millihertz. The coronal dissipation coefficient is estimated to be eight to nine orders of magnitude larger than the theoretically predicted classical value. The larger dissipation coefficient may solve existing difficulties with wave heating and reconnection theories.

One of the main scientific objectives of the TRACE spacecraft (*1*) is to investigate the mechanisms of the heating of the outer solar atmosphere. The understanding of the mechanism of coronal heating is important not only in the context of solar atmospheric physics but also in relation to the sun-Earth connection, in examining the influence of the expanding hot solar corona on the interplanetary and near-Earth space environments. The expanding solar atmosphere forms the solar wind that during peaks of solar activity can cause magnetic storms by perturbing Earth's magnetosphere, damaging satellites, affecting communications, and even inducing power outages in ground-based electrical grids.

Flares may generate fast wave pulsations in coronal loops (*2, 3*). Oscillations in coronal loops were recently observed by TRACE, and Aschwanden *et al.* (*4*) have reported spatial oscillations of coronal loops. The spatial oscillations were detected by TRACE in five loops with periods ranging from 258 to 320 s and were interpreted as kink mode magnetohydrodynamic (MHD) standing waves. The oscillating loops show evidence of strong damping (that is, the amplitude of the oscillations decreases by more than 50% in several oscillation periods). However, the damping was not analyzed in (*4*). Here we present the observations and analysis of damped magnetic loop oscillations induced by a flare in the solar corona.

The dissipation coefficient and the spatial scale at which the dissipation occurs help determine the coronal heating mechanism. Heating of coronal loops may occur by trapped Alfvén waves (*5*), or by reconnection of entangled magnetic field (*6*). The theoretical classical value of the dissipation coefficient is determined by viscosity (*7*) and resistivity (*8*) with the appropriate dissipation scale in a laminar coronal plasma. The classical dissipation coefficient is too low to account for the required heating rate necessary to explain observed coronal temperatures of ~10^6 K with wave heating (*9–11*) or reconnection (*9*) models.

We consider the evolution of the loop position in images taken by TRACE (Fig. 1) with almost constant cadence of ~75 s and an exposure time of about 16.4 s. The analyzed sequence of 88 images of active region AR8270 began at 12:11 UT, on 14 July 1998 (*12*). The data were initially preprocessed: the dark current and the artificial offset were subtracted from each image, and the images were normalized for variations in the exposure time. A movie created from these images shows the onset of loop oscillations after the flare, which occurred at about 12:55 UT. The oscillations were observed to damp within a few oscillation periods. In the movie it is apparent that there is a large set of loops that undergo damped oscillations after the flare. These loops are closely spaced (the maximal separation is several million meters) and originate in the vicinity of the flare site. For simplicity, we have chosen to analyze an isolated loop (outlined in Fig. 1) at about 80 × 10^6 m from the flare site.

For the analysis, we took four horizontal cuts nearly perpendicular to the loop axis close to the loop apex. To improve the signal-to-noise ratio, we averaged the intensity in the four adjacent cuts. We found good correlation of loop motions between the cuts. In-phase motion of the loop is evident in the movie sequence of the post flare loop oscillations (*12*). Such in-phase displacement of the loop suggests that the oscillations correspond to the global mode. The global mode occurs when the loop acts as a resonant cavity for transverse MHD waves, and all parts of the loop oscillate in phase. The MHD waves are trapped in the loop and no significant wave leakage can occur (*10, 13–16*). The trapped waves may dissipate by viscous dissipation of velocity gradients (*10, 11, 17*) or by resistive dissipation of currents generated by magnetic field gradients (*13–16*) in the loop. The above two mechanisms are expected to lead to dissipation of the low-frequency

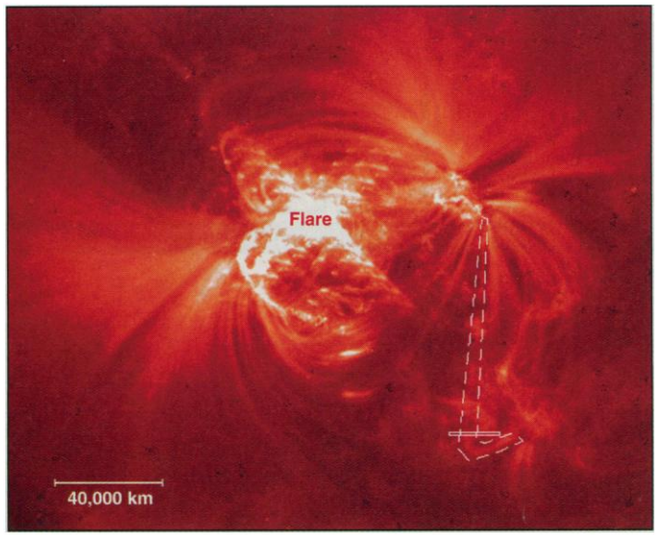

Fig. 1. The coronal loop system observed with TRACE. The flare site is marked and the analyzed oscillating loop is outlined. The box marks the location of the four cuts. The pointing of the image center is (−284 arc sec, −363 arc sec) from the sun center. The image size is 768 by 768 pixels, with a pixel size of 0.5 arc sec (360 km).

[1]School of Mathematical and Computational Sciences, University of St. Andrews, St. Andrews, Fife KY16 9SS, Scotland. [2]Raytheon ITSS/NASA Goddard Space Flight Center, 682, Greenbelt, MD 20771, USA. [3]Harvard-Smithsonian Center for Astrophysics, Cambridge, MA 02138, USA. [4]NASA Goddard Space Flight Center, 682, Greenbelt, MD 20771, USA.

*To whom correspondence should be addressed. E-mail: leon.ofman@gsfc.nasa.gov

wave in the collision-dominated plasma of the active region loop.

The temporal dependence of the loop displacement is displayed by plotting the horizontal coordinate (in kilometers) of the maximum intensity across the loop as a function of time. The temporal evolution of the loop displacement calculated as an average coordinate of the loop position for four neighboring perpendicular cuts (Fig. 2) is fitted by

$$A(t) = A_0 \sin(\omega t + \phi) e^{-\lambda t} \quad (1)$$

where the displacement amplitude A_0 = 2030 ± 580 km, oscillation frequency ω = 1.47 ± 0.05 rad min^{-1}, the phase $\phi = -1.0 \pm 0.34$ rad, and the decay rate $\lambda = 0.083 \pm 0.046$ min^{-1}. These parameters yield a frequency of 3.90 ± 0.13 mHz and a decay time 12.1 ± 6.7 min for the loop oscillations. A less conservative error bar for the decay time may be obtained by dividing the time sequence into 10 shorter overlapping sections and calculating the decay rate of the sections. With this method we obtain $\lambda = 0.069 \pm 0.013$ min^{-1}, where the range is obtained from the maximal and the minimal decay rates of the sections. The corresponding decay time is 14.5 ± 2.7 min. From the time-derivative of Eq. (1), the estimated peak loop velocity is 47 ± 14 km s^{-1}. We estimated the footpoint leakage (*18*) in this loop and found that the leakage time is nearly two orders of magnitude longer than the measured decay time of the loop oscillations.

The in-phase displacement of the loop near its apex is caused by a global kink mode of the loop (Fig. 3). This is a normal mode of the loop in which all parts of the loop oscillate transversely and in phase. The wavelength of the mode is double the length of the loop, and nodes of the mode coincide with the loop footpoints. From the measured distance between the footpoints [(83 ± 4) × 10^6 m], we calculated the loop length (as a semicircular arc) $L = (130 \pm 6) \times 10^6$ m. Neglecting the effects of gravity and loop curvature (which are not expected to significantly affect our results) and approximating the loop as a uniform flux tube embedded in a uniform magnetic field, we can describe the mode by the relation (*2, 19*)

$$f = \frac{C_k}{2L}, \quad C_k = \left(\frac{2}{1 + \rho_o/\rho_i}\right)^{1/2} C_A \quad (2)$$

where C_A is the Alfvén speed inside the loop, C_k is the speed of propagation of the kink mode, and ρ_i and ρ_o are the plasma densities inside and outside the loop, respectively. For the period and length observed, we obtain C_k = 1040 ± 50 km s^{-1}. Assuming an order of magnitude density enhancement for a typical coronal loop, that is, $\rho_o/\rho_i \sim 0.1$, we obtain $C_A \approx 770 \pm 40$ km s^{-1}. In our analysis we assumed that the loop's half-width is much less than L, and this is justified by the observations. Using the deduced Alfvén speed and the observed loop half-width, we estimate an Alfvén crossing time τ_A = 1.3 s.

The observed dissipation of the resonant global mode may be due to viscous and resistive dissipation that have a similar effect on the wave dissipation (*10, 17*). The dependence of the wave amplitude decay rate on the resistive dissipation coefficient is well known (*13, 14, 20*). The effect of viscous dissipation on the resonant absorption of the global mode has been investigated in detail by Ofman, Davila, and Steinolfson (*17*) who solved the linearized time-dependent visco-resistive MHD equations, with the loop approximated by a slab of magnetized plasma.

Viscous dissipation in a fluid is expressed in terms of the dimensionless Reynolds number R. Similarly, the magnetic diffusion coefficient gives rise to the dimensionless magnetic Reynolds number (or the Lundquist number) S. Using the decay rate deduced from the observed loop $\tau_d \equiv \lambda^{-1} = 14.5 \pm 2.7$ min = (600 ± 110)τ_A and assuming that the dissipation is dominated by viscosity, we apply the scaling law $\tau_d = c_v R^{0.22}$, where the constant $c_v = 32.6\tau_A$ and the power index 0.22 were calculated numerically for the fundamental mode ($k_z = 2L$) using the model described in (*17*). In this calculation, the loop is perturbed by a pulse perpendicular to the magnetic field at time $t = 0$. The induced wave motions were dominated by the resonant global mode oscillations for the particular loop geometry that dissipated at a rate determined by the viscosity.

Using the calculated decay rate dependence on R (Fig. 4) and the observed decay rate we estimated $R = 10^{5.3-6.1}$. The Reynolds number deduced from the observations is eight to nine orders of magnitude smaller than the classical value of $R = 10^{14}$. Similarly, assuming that the dissipation is dominated by the plasma resistivity, we applied the scaling law $\tau_d = c_r S^{0.22}$, where the constant $c_r = 38.5\tau_A$ and the power law index 0.22 were calculated numerically (*20*). Using the resistive power law, we estimate a Lundquist number $S = 10^{5.0-5.8}$. S is seven to eight orders of magnitude smaller than the commonly quoted (*21*) classical value of $S = 10^{13}$.

The waves are dissipated so efficiently inside the loop because of the global mode resonance and the formation of a narrow dissipation layer inside the loop. The width of the resonance dissipation layer scales as $R^{-1/3}$ (*11, 17*) [$S^{-1/3}$ for resistive dissipation (*22*)], and it is ~15 km in the observed loop, significantly below the resolution of TRACE (~360 km at center to ~400 km near the limb of the sun). The velocity gradients in the resonance dissipation layer scale as $R^{2/3}$ (*17*). Thus, the velocity gradients in the resonance layer are more than three orders of magnitude larger than the velocity gradients between the loop and the outside medium (assuming the velocity gradient between the loop and the outside medium is independent of R). Because the shear viscous dissipation is proportional to the square of the velocity gradient, most of the dissipation will occur inside the loop (*17*).

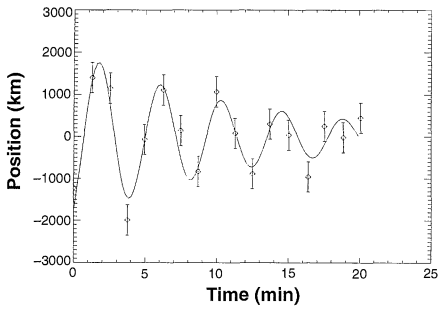

Fig. 2. The temporal evolution of the loop displacement calculated as an average coordinate of the loop position for four neighboring perpendicular cuts through the loop apex (diamonds), with error bars (±0.5 pixel) starting at 13:13:51 UT on 14 July 1998. The solid curve is the best fit function (*1*). The effect of the image motion through the field of view was subtracted in this analysis.

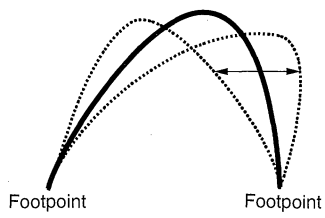

Fig. 3. A sketch of a coronal loop that undergoes global mode oscillations. The dominant magnetic field component is along the loop axis. The oscillations are transverse to the direction of the magnetic field. The loop's footpoints are anchored in the dense photosphere-chromosphere.

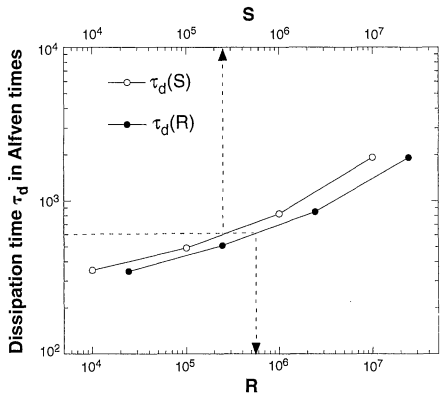

Fig. 4. The dependence of the dissipation time (in Alfvén times) on the dimensionless Reynolds number R and the Lundquist number S for the fundamental global mode in the model of the observed loop. The oscillation decay time and the corresponding R and S are marked by the dashed lines and arrows.

The index of the calculated viscous and resistive power laws is close to the 1/5 found by Poedts and Kerner (*13*) for resistive dissipation in a cylindrical loop. We found that the power law index increases when R or $S > 10^6$ (Fig. 4), in agreement with (*20*), which means that with the classical values of S and R the estimated dissipation time would be at least three orders of magnitude longer than the observed dissipation time.

The decay of the loop oscillation amplitude indicates the presence of strong dissipation of the wave energy. Dissipation leads to the heating of coronal loops. We found that as the oscillations are dissipated, the loop dims in the cooler 171 Å line (1.3×10^6 K ionization temperature), and appears to brighten in the hotter 195 Å line (1.6×10^6 K ionization temperature). This process is consistent with our understanding of the dissipation process and needs further detailed study.

If mainly the viscosity is enhanced compared with the classical value, then our results favor coronal heating by viscous dissipation of waves. Numerical simulations indicate that the classical viscosity may be enhanced by small-scale turbulence driven by fluid instabilities of the coronal plasma (*23–25*), in agreement with theoretical predictions (*9, 11*). Similarly, the enhancement of resistive dissipation requires the formation of turbulent current eddies at small spatial scales (*9*) (which in our view is less favorable for coronal loop conditions, because of the small growth rate of current instabilities compared with fluid instabilities). If the resistivity is enhanced (or the resistivity and the viscosity are enhanced), then our results support the dissipation of waves and the magnetic reconnection mechanisms for coronal heating. The difficulties that arise in these models, when the classical value of the dissipation coefficient is used, are eliminated. The fundamental plasma parameters in the solar corona are relevant to the understanding of the solar flares, to the acceleration of the solar wind and coronal mass ejection, and, ultimately, to the sun-Earth connection.

References and Notes

1. The TRACE spacecraft contains a 30-cm diameter telescope with 8.66-m Cassegrain focal length. The optics consists of superpolished mirrors individually coated in four quadrants to allow observations of the three extreme ultraviolet emission lines of 171 Å (Fe^{IX}), 195 Å (Fe^{XII}), and 284 Å (Fe^{XV}), and between 1200 and 7000 Å. Focal plane filters allow TRACE to select ultraviolet passbands around Lyman-α (1216 Å), C IV (1550 Å), the ultraviolet continuum at 1600 Å and 1700 Å, and the visible continuum up to 7000 Å wavelengths (*26*). Additional detail on the TRACE spacecraft can be found in Handy *et al.* (*27*) and at http://vestige.lmsal.com/TRACE/. First results from the TRACE mission are reported by Schrijver *et al.* (*28*) and by Golub *et al.* (*29*).
2. B. Roberts, P. M. Edwin, A. O. Benz, *Nature* **305**, 688 (1983).
3. ———, *Astrophys. J.* **279**, 857 (1984).
4. M. J. Aschwanden, L. Fletcher, C. Schrijver, D. Alexander, *ibid.*, in press.
5. J. A. Ionson, *ibid.* **226**, 650 (1978).
6. E. N. Parker, *ibid.* **264**, 642 (1983).
7. S. I. Braginskii, *Rev. Plasma Phys.* **1**, 205 (1965).
8. L. Spitzer Jr., *Physics of Fully Ionized Gases* (Interscience, New York, 1962).
9. J. Heyvaerts and E. R. Priest, *Astron. Astrophys.* **117**, 220 (1983).
10. J. M. Davila, *Astrophys. J.* **317**, 514 (1987).
11. J. V. Hollweg and G. Yang, *J. Geophys. Res.* **93**, 5423 (1988).
12. A movie made from these images is available as supplementary material at www.sciencemag.org/feature/data/1040166.shl.
13. S. Poedts and W. Kerner, *Phys Rev. Lett.* **66**, 2871 (1991).
14. R. S. Steinolfson and J. M. Davila, *Astrophys. J.* **415**, 354 (1993).
15. L. Ofman, J. M. Davila, R. S. Steinolfson, *ibid.* **444**, 471 (1995).
16. W. J. Tirry and M. Goossens, *ibid.* **471**, 501 (1996).
17. L. Ofman, J. M. Davila, R. S. Steinolfson, *ibid.* **421**, 360 (1994).
18. D. Berghmans and P. De Bruyne, *ibid.* **453**, 495 (1995).
19. P. M. Edwin and B. Roberts, *Sol. Phys.* **88**, 179 (1983).
20. L. Ofman and Z. Mouradian, *Astron. Astrophys.* **308**, 631 (1996).
21. L. Golub and J. M. Pasachoff, *The Solar Corona* (Cambridge Univ. Press, Cambridge, 1997), p. 219.
22. J. M. Kappraff and J. A. Tataronis, *J. Plasma Phys.* **18**, 209 (1977).
23. J. T. Karpen, R. B. Dahlburg, and J. M. Davila, *Astrophys. J.* **421**, 372 (1994).
24. L. Ofman, J. M. Davila, R. S. Steinolfson, *Geophys. Res. Lett.* **21**, 2259 (1994).
25. L. Ofman and J. M. Davila, *J. Geophys. Res.* **100**, 23427 (1995).
26. The optics contains an active secondary mirror with image motion compensation. Pointing is internally stabilized to 0.1 arc sec against spacecraft jitters. A 1024 by 1024 charge-coupled device (CCD) detector collects images over an 8.5 arc min by 8.5 arc min field-of-view. A powerful data handling computer enables flexible use of the CCD array including adaptive target selection, data compression, and fast operation for a limited field-of-view.
27. B. N. Handy *et al.*, *Sol. Phys.* **183**, 29 (1998).
28. C. J. Schrijver *et al.*, *ibid.*, in press.
29. L. Golub *et al.*, *Rev. Plasma Phys.*, in press.

30. We thank the TRACE team. L.O. acknowledges support by the NASA Solar Physics Supporting Research and Technology program, the NASA Space Physics Theory Program, and the NASA High-Performance Computing and Communications program. E.E.D. was supported by contract NAS5-38099 with NASA Goddard Space Flight Center. V.M.N. and B.R. acknowledge Particle Physics and Astronomy Research Council support.

18 March 1999; accepted 7 June 1999

Minimum Field Strength in Precessional Magnetization Reversal

C. H. Back,[1]* R. Allenspach,[2] W. Weber,[1] S. S. P. Parkin,[3] D. Weller,[3] E. L. Garwin,[4] H. C. Siegmann[1]

Ultrafast magnetic field pulses as short as 2 picoseconds are able to reverse the magnetization in thin, in-plane, magnetized cobalt films. The field pulses are applied in the plane of the film, and their direction encompasses all angles with the magnetization. At a right angle to the magnetization, maximum torque is exerted on the spins. In this geometry, a precessional magnetization reversal can be triggered by fields as small as 184 kiloamperes per meter. Applications in future ultrafast magnetic recording schemes can be foreseen.

Based on experimental advances, magnetization reversal has undergone considerable development in recent years. For instance, it is now possible to observe the direction of the magnetization in nanosized single-domain particles (*1–3*). In such experiments, static magnetic fields are applied. The probability that the magnetization $\vec{M}$ will reverse is determined as a function of the angle at which the external magnetic field $\vec{H}_{ex}$ is applied to the particle. The reversal mechanism is difficult to understand in detail, because $\vec{M}$ can assume complex curling and buckling modes depending on the details of the shape and magnetic properties of the particle. A conceptually simpler reversal mode is reversal by precession of the magnetization: No curling and buckling modes occur (*4, 5*). Precessional and conventional reversal differ in the angle between $\vec{M}$ and $\vec{H}_{ex}$ and in the duration of the applied field pulse. In conventional magnetic recording, for example, the reversing field is applied antiparallel to the direction of $\vec{M}$, limiting the reversal speed to the nanosecond level (*6, 7*). Much shorter reversal times can be achieved if the external magnetic field inducing the reversal is applied perpendicular to $\vec{M}$ (*4*). In this case, the magnetic field pulse induces a precessional motion of the magnetization vector that leads to magnetization reversal. Precessional reversal in the picosecond regime was demonstrated for thin films magnetized perpendicular to the film plane. However, the magnetic field had to exceed ≈2000 kA/m at a pulse length of a few pico-

[1]Laboratorium für Festkörperphysik, ETH Zürich, CH-8093 Zürich, Switzerland. [2]IBM Research Division, Zurich Research Laboratory, CH-8803 Rüschlikon, Switzerland. [3]IBM Research Division, Almaden Research Center, 650 Harry Road, San Jose, CA 95120, USA. [4]Stanford Linear Accelerator Center, Stanford University, Stanford, CA 94305, USA.

*To whom correspondence should be addressed. E-mail: back@solid.phys.ethz.ch